

# Rest Myocardial Perfusion/Metabolism Imaging Using Simultaneous Dual-Isotope Acquisition SPECT with Technetium-99m-MIBI/Fluorine-18-FDG

Dominique Delbeke, Searle Videlefsky, James A. Patton, Michelle G. Campbell, William H. Martin, Israel Ohana and Martin P. Sandler

*Section of Nuclear Medicine, Department of Radiology and Radiological Sciences, Department of Medicine/Cardiology, Vanderbilt University Medical Center, Nashville, Tennessee; and Elscint, Inc., Haifa, Israel*

The purpose of this study was to develop a dual-isotope simultaneous acquisition (DISA) protocol using a multihead SPECT camera equipped with an ultrahigh-energy (UHE) collimator to evaluate simultaneously rest cardiac perfusion and metabolism with  $^{99m}\text{Tc}$ -MIBI/ $^{18}\text{F}$ FDG. **Methods:** Physical measurements were first performed with phantoms to develop the acquisition protocol. Fifteen patients underwent DISA-SPECT with  $^{99m}\text{Tc}$ -MIBI/ $^{18}\text{F}$ FDG to validate the protocol. To evaluate the quality of the  $^{99m}\text{Tc}$ -MIBI images acquired with the UHE collimator, four patients underwent a resting  $^{99m}\text{Tc}$ -MIBI scan acquired with a high-resolution, low-energy collimator prior to DISA-SPECT. **Results:** With a window of 20% for both photopeaks and a  $^{99m}\text{Tc}$ / $^{18}\text{F}$  concentration ratio of 3.2:1, the spillover from  $^{18}\text{F}$  into the  $^{99m}\text{Tc}$  window is 6% of the counts in the window for normal subjects. Phantom images clearly demonstrated defects measuring  $2 \times 1$  and  $2 \times 0.5$  cm. Technetium-99m-MIBI images obtained with the UHE and high-resolution collimators provided similar diagnostic information. Using a stenosis of >70% as criteria to diagnose coronary artery disease, DISA-SPECT had a sensitivity of 100% and a positive predictive value of 93%. **Conclusion:** Simultaneous evaluation of rest myocardial perfusion/metabolism with a multihead SPECT camera equipped with an UHE collimator is possible using  $^{99m}\text{Tc}$ -MIBI/ $^{18}\text{F}$ FDG with a dual-isotope simultaneous acquisition protocol.

**Key Words:** technetium-99m-MIBI; fluorine-18-FDG; single-photon emission computed tomography; dual-isotope acquisition

**J Nucl Med 1995; 36:2110–2119**

**T**he identification of injured but viable myocardium in patients with poor ventricular function has become increasingly important as investigators have demonstrated an im-

provement in ventricular performance in patients with hibernating myocardium who undergo surgical revascularization (1–8). Hibernating myocardium has impaired contractility secondary to chronic hypoperfusion; however, metabolism is preserved producing a perfusion/metabolism mismatch, and recovery of function can occur following revascularization (9). Conversely, if the myocardium is infarcted, the decreased perfusion will result in a loss of metabolic activity resulting in a matched perfusion/metabolism defect, and impairment of contractile function is permanent.

Myocardial perfusion can be evaluated with  $^{201}\text{Tl}$ -chloride,  $^{99m}\text{Tc}$ -2-hexakis-2-methoxy-2-methylpropyl isonitrile ( $^{99m}\text{Tc}$ -MIBI) SPECT or  $^{13}\text{N}$ -ammonia and PET. PET, however, used to be the only modality to allow direct evaluation of metabolism. Evaluation of glucose metabolism using  $^{18}\text{F}$ fluorodeoxyglucose ( $^{18}\text{F}$ FDG) remains the gold standard to evaluate myocardial viability.

Recent modification of  $^{201}\text{Tl}$  protocols, which include 24-hr delayed images (10) or imaging after reinjection of  $^{201}\text{Tl}$  (11–14), has improved the detection of viable myocardium when PET is not available. These protocols, however, have been shown to underestimate myocardial viability (15–18).

Several groups have demonstrated that  $^{18}\text{F}$ FDG cardiac images obtained with a SPECT camera equipped with an ultra-high energy collimator provide clinical information equivalent to that obtained with PET (19–24).

Although the feasibility of imaging  $^{18}\text{F}$ FDG with SPECT has been demonstrated, the protocols still require separate acquisitions for perfusion/metabolism images and are thus associated with the disadvantage of a double-acquisition study. The purpose of this study was to develop a dual-isotope simultaneous acquisition protocol (DISA) using a multihead SPECT camera equipped with ultra-high energy (UHE) collimators to evaluate rest cardiac perfusion/metabolism with  $^{99m}\text{Tc}$ -MIBI/ $^{18}\text{F}$ FDG.

Received Dec. 27, 1994; revision accepted Jun. 20, 1995.

For correspondence or reprints contact: Martin P. Sandler, MD, Department of Radiology and Radiological Sciences, Vanderbilt University Medical Center, 21st Avenue South & Garland, Nashville, TN 37232-2675.

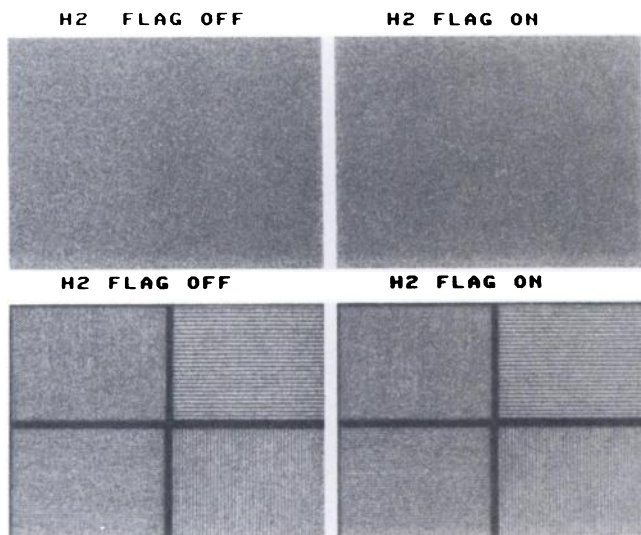


**FIGURE 1.** Corrected intrinsic uniformity and bar pattern measurements (3 million counts) obtained in the regular (H2 flag off) and high-energy modes (H2 flag on). Only a slight difference in integral uniformity was measured (3.40%–3.72%) and no difference in spatial resolution was observed.

## MATERIALS AND METHODS

### Equipment and Physical Dual-Isotope Measurements

SPECT imaging was performed using the Apex Helix (Elsint Inc) dual-head, rectangular field of view digital scintillation camera. The camera was modified by the manufacturer to permit imaging of the 511-keV photons from positron emitters in the singles mode only. First, a software selectable, high-energy mode switch was installed, permitting a change in energy range from 30–400 keV to 100–560 keV and facilitating the extension of the medium-energy linearity maps into the high-energy range. Extrinsic sensitivity maps (30 million counts) with  $^{99m}\text{Tc}$  and  $^{18}\text{F}$  were obtained to correct for nonuniformities in the camera/high-energy collimator combination. These modifications preserved the spatial resolution and uniformity characteristics of the routine mode of operation with low-energy photon emitters as shown in Figure 1. These changes resulted in a measured energy resolution of 8.5% (FWHM of photopeak) at 511 keV, while maintaining an energy resolution of 11% at 140 keV. At this energy, the 3/8-in. thick NaI crystals have a photopeak detection efficiency of approximately 13%.

A set of UHE collimators was designed to support ultrahigh-energy, general-purpose, whole-body and SPECT applications. The detailed characteristics of these collimators for imaging 511 keV photons have been reported previously (20). To determine the imaging characteristics of the system with the UHE collimator at 140 keV, line spread functions were measured with a thin line source of  $^{99m}\text{Tc}$  in air at multiple distances utilizing an energy window of 140 keV  $\pm 10\%$ . Plane source sensitivity of the system was also measured using a 10-cm disk source of  $^{99m}\text{Tc}$  following the NEMA sensitivity protocol. Line spread function and plane source sensitivity measurements were also made with  $^{99m}\text{Tc}$  using a low-energy, high-resolution (LEHR) collimator for comparison purposes (Table 1).

SPECT spatial resolution measurements with scatter were made with a line source of  $^{99m}\text{Tc}$  in the center of a 22-cm water-filled cylindrical phantom using a 13-cm radius of rotation and

**TABLE 1**  
Planar Spatial Resolution and Sensitivity

Collimator	Isotope	Spatial resolution FWHM (mm) at 10 cm in air	Sensitivity (cpm/ $\mu\text{Ci}$ )
UHE	$^{18}\text{F}$	14.5	129
UHE	$^{99m}\text{Tc}$	11.1	114
LEHR	$^{99m}\text{Tc}$	8.4	160

UHE = ultrahigh energy; LEHR = low-energy high resolution.

circular orbit. A ramp filter was used for image reconstruction to optimize spatial resolution measurements. SPECT volume sensitivity measurements using both heads were made with a 22-cm cylindrical phantom containing a solution of  $^{99m}\text{Tc}$  and using a 13-cm radius of rotation and a circular orbit.

Image acquisitions of 30 min duration were performed with the SPECT system using a cardiac phantom containing 300  $\mu\text{Ci}$   $^{18}\text{F}$  and placed in a 22-cm diameter water-filled cylindrical phantom. A 13-cm radius of rotation was used for SPECT imaging. The phantom contained two simulated 45° defects: one 2  $\times$  1 cm and the other 2  $\times$  0.5 cm. Data were collected from both heads of the camera system using the dual-isotope technique, which enables simultaneous but separate acquisition in two energy windows, and 180° rotation.

SPECT reconstruction was accomplished from the  $^{18}\text{F}$  window for the single anterior detector alone (180° acquisition) and for both detectors together (360° acquisition) by using a ramp filter multiplied by a Butterworth filter with a cutoff of 0.35 (cycles/pixel) and an order of 5. Image comparisons were performed to determine the optimum acquisition protocol. In addition, SPECT image reconstruction was also accomplished from the  $^{99m}\text{Tc}$  window to evaluate the contribution of downscatter from  $^{18}\text{F}$  into the  $^{99m}\text{Tc}$  window. Total counts from the heart phantom were determined for both windows. A solution of  $^{99m}\text{Tc}$  was then added to the phantom and the dual-isotope SPECT image acquisition was repeated. The activity of  $^{99m}\text{Tc}$  was calculated to provide a ratio of 3.2:1 in comparison to  $^{18}\text{F}$  to simulate the ratio of activities in the myocardium at the time of imaging following the dual-isotope SPECT protocol. This ratio was calculated by decaying the administered doses of  $^{18}\text{F}$  and  $^{99m}\text{Tc}$  to the start of the acquisition in the clinical protocol and assuming identical percent uptakes for the two radiopharmaceuticals. Technetium-99m images were also reconstructed using a ramp filter multiplied by a Butterworth filter but with a cutoff of 0.45 (cycles/pixel) and an order of 5. Reconstructed SPECT images were compared for the two windows to evaluate the potential diagnostic quality of the dual-isotope technique with the UHE collimator.

Total counts from the heart for the two windows were determined in five different patients who underwent imaging using the dual-isotope protocol and were reported as having normal distributions of both radiopharmaceuticals (confirmed by coronary angiography) to determine the contribution of downscatter from  $^{18}\text{F}$  to the  $^{99m}\text{Tc}$  window for normal global perfusion and metabolism.

An additional set of phantom data was obtained to evaluate the effects of  $^{18}\text{F}$  downscatter in a region of myocardial ischemia where the global perfusion is reduced and metabolism is increased. Two centimeter diameter vials were filled with solutions of  $^{99m}\text{Tc}$  and  $^{18}\text{F}$  to simulate normal ( $^{99m}\text{Tc}/^{18}\text{F} = 3.2/1$ ), 75% normal ( $^{99m}\text{Tc}/^{18}\text{F} = 2.4/1$ ), 50% normal ( $^{99m}\text{Tc}/^{18}\text{F} = 1.6/1$ ) and 25%

**TABLE 2**  
Clinical and Imaging Data

Patient no.	Age (yr)	Sex	Known MI	EF(%)	Wall motion by left ventriculogram and echocardiography	Defect*	Angiography
1	57	M	Anterior	15	AK:12389 HK: 4	M:123489	LAD >70%
2	76	M	Inferior	20	HK:global	M:123 M: 45	LAD 100% RCA 100%
3	43	F	na	na	na	M:27 Mis: 13456	na
4	68	M	None	60	Normal	Mis:67	LCx >70%
5	54	M	Inferior (nonQ)	60	Normal	Mis:467	LCx >70%
6	34	M	Anterior	35	AK:12389 AK: 45	M:123 M: 45	LAD >70% RCA 100%
7	68	M	None	48	AK: 45 HK: global	Mis: 45	Normal
8	59	M	Inferior	25	AK: 145 HK: 2389	M:145	RCA 100% LAD >70%
9	80	F	None	25	HK: 12389 HK: 45	Mis: 12389 Mis: 45	LAD 100% RCA 100%
10	72	F	Inferior	70	Normal	Mis: 45	LCx >70%
11	48	M	Anterior	20	HK: 12389 HK: 45	M: 12389 M: 45	LAD 100% RCA 100%
12	52	M	Anteroseptal	35	AK: 12389	M: 12389	Left main 100%
13	64	M	Anteroseptal	20	AK: 123 HK: 45	M: 1238 M: 45	LAD 100% RCA 100%
14	47	M	Anterior	20	HK: global	M: 1238 Mis: 9	LAD 100%
15	82	M	Inferior None	20	HK: global	M: 45 Mis: 289 M: 1 Mis: 45	RCA 100% LAD >70% RCA 100%

\*Defect: see Figure 3 for segmental location.

AK = akinesis; HK = hypokinesis; EF = ejection fraction; na = not available; M = matched defect, MIS = mismatched defect; LAD = left anterior descending; LCx = left circumflex; RCA = right coronary artery; Left = left main; MI = myocardial infarction.

normal ( $^{99m}\text{Tc}/^{18}\text{F} = 0.8/1$ ) global perfusion (vial A). For each of these conditions, additional vials were filled with solutions of  $^{99m}\text{Tc}$  and  $^{18}\text{F}$  to represent regions of 100%, 75%, 50%, 25% and 0% ischemia (vial B). A constant activity of  $^{18}\text{F}$  (100  $\mu\text{Ci}$ ) was present in all vials representing normal myocardial metabolism. These vials were then imaged at a constant time using the dual-isotope technique and  $^{99m}\text{Tc}$  window counts were determined from each vial using a circular region of interest that just included the vial. Data from these samples were used to determine net counts per microcorie from  $^{99m}\text{Tc}$  and  $^{18}\text{F}$  appearing in the  $^{99m}\text{Tc}$  window. These values were then used to generate four graphs of calculated percentage of contrast [ $(^{99m}\text{Tc}$  window counts in simulated region of ischemia (B)/ $^{99m}\text{Tc}$  window counts in simulated myocardium (A)  $\times$  100) versus actual % contrast ( $(^{99m}\text{Tc}$  activity in B/ $^{99m}\text{Tc}$  activity in A)  $\times$  100] for normal to 25% of normal global perfusion. A range of 0 to 4 times normal metabolism ( $^{18}\text{F}$ ) was simulated in each graph.

#### Patients

Fifteen patients referred for evaluation of dysfunctional but viable myocardium underwent DISA-SPECT with  $^{99m}\text{Tc}$ -MIBI/ $^{18}\text{F}$ FDG.

Four patients underwent  $^{99m}\text{Tc}$ -MIBI imaging with a LEHR collimator prior to glucose loading and  $^{18}\text{F}$ FDG administration, using the same acquisition parameters as for the dual-isotope protocol. These patients then underwent DISA-SPECT using the UHE collimators.

The data for the 15 patients included in the study are summarized in Table 2. There were 12 men and 3 women with an average age  $60 \pm 14$  yr. The average left ventricular ejection fraction (LVEF) was  $34\% \pm 17\%$ . One patient was an insulin-dependent diabetic. Patients were not instructed to discontinue taking cardiac medication, including beta-blocking agents and calcium antagonists. Fourteen patients underwent coronary angiography within 3 mo of their scintigraphic evaluation. This protocol was approved by the VUMC Institutional Review Board and all participants gave written informed consent.

#### Dual-Isotope Single Acquisition SPECT

The schematic protocol for DISA-SPECT using  $^{18}\text{F}$ FDG and  $^{99m}\text{Tc}$ -MIBI is shown in Figure 2. Patients fasted for a minimum of 4 hr prior to the study. With the exception of the patient with insulin-dependent diabetes, all patients were loaded with 50 g oral glucose approximately 60 min prior to intravenous injection of 370

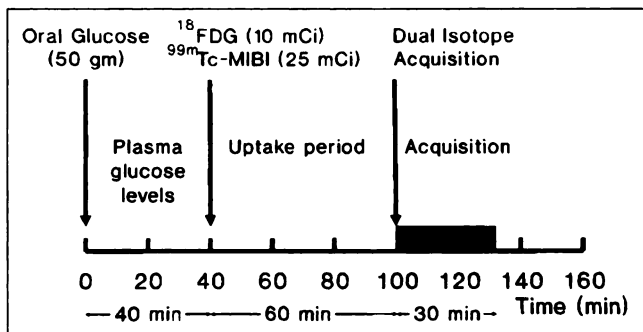


**FIGURE 2.** Protocol for identifying injured but viable myocardium with DISA-SPECT using  $^{99m}\text{Tc}$  MIBI/ $^{18}\text{F}$  FDG.

MBq (10 mCi)  $^{18}\text{F}$  FDG and 925 MBq (25 mCi)  $^{99m}\text{Tc}$ -MIBI. Soluble insulin was administered intravenously, if required, according to blood glucose levels. After a 60-min uptake phase, the patients underwent DISA-SPECT.

Data acquisition was accomplished by positioning two 20% pulse-height analyzer windows symmetrically about the 140-keV photopeak of  $^{99m}\text{Tc}$  and the 511-keV photopeak of  $^{18}\text{F}$ . The digital electronics of the camera permitted frame-by-frame decay correction for short-lived radioisotopes such as  $^{18}\text{F}$ .

The acquisition protocol included a single-head rotating  $180^\circ$  from the right anterior oblique to the left posterior oblique projection for 60 stops ( $3^\circ$  between stops) at 30 sec/stop. The images from the two windows were collected in separate  $64 \times 64$  matrices using word mode and then reconstructed using a ramp filter multiplied by a Butterworth filter with a cutoff of 0.3 to 0.5 (cycles/pixel) and an order of 5, followed by spatial smoothing along the short-axis, horizontal long-axis and vertical long-axis of the heart. Thus, two separate sets of slices mapping the  $^{99m}\text{Tc}$ -MIBI and  $^{18}\text{F}$  FDG distributions were simultaneously obtained, resulting in one-to-one correspondence in spatial registration.

### Image Analysis

SPECT slices were reoriented perpendicularly to the short-axis of the heart. Two sets of short-axis images from  $^{99m}\text{Tc}$ -MIBI and  $^{18}\text{F}$  FDG-SPECT were compared side-by-side separately by two independent experienced observers without prior knowledge of cardiac angiography between the two observers.

Qualitative analysis was performed using a nine-segment model per study (Fig. 3): an apical segment as well as distal and proximal (basal) segments of the anterior, inferior, lateral and septal walls. Segments were classified into three categories: normal, good  $^{18}\text{F}$  FDG and  $^{99m}\text{Tc}$ -MIBI uptake; mismatched defect, moderate to severe decreased uptake of  $^{99m}\text{Tc}$ -MIBI but adequate  $^{18}\text{F}$  FDG uptake, suggesting hibernating myocardium; and matched defects, moderate to severe decreased uptake of both  $^{99m}\text{Tc}$ -MIBI and  $^{18}\text{F}$  FDG indicative of scar.

### Coronary Angiography

Angiograms were obtained in multiple orthogonal projections and single and biplane left ventriculography was performed. Cineangiograms were assessed by an experienced angiographer unaware of both the clinical and scintigraphic data. Extent of coronary artery disease (CAD) was defined as number of vessels with a stenosis  $>70\%$ , or, for patients with coronary artery bypass graft (CABG), both the native vessel as well as the graft supplying that vascular distribution required  $>70\%$  stenosis for consideration as a hemodynamically significant stenosis.

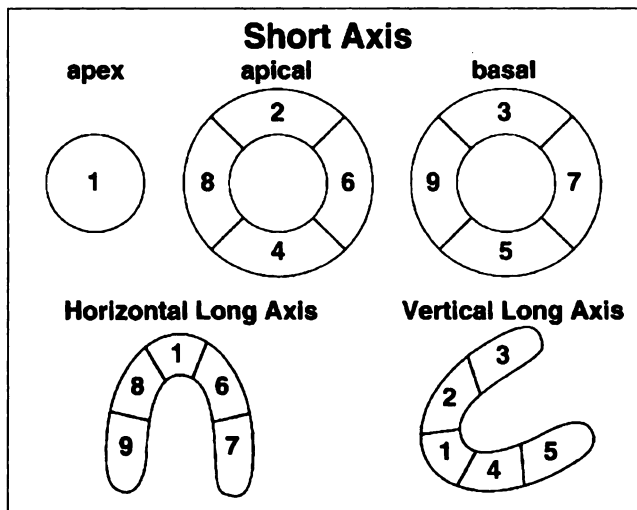


**FIGURE 3.** Schematic presentation of nine segments per study.

### Data Interpretation

The ability of  $^{99m}\text{Tc}$ -MIBI/ $^{18}\text{F}$  FDG DISA-SPECT to predict involvement of individual coronary vessels was assessed by ascribing the septum and anterior walls to the left anterior descending (LAD) coronary artery; the lateral wall to the circumflex artery; and the inferior wall to the right coronary artery (RCA), except in patients in whom coronary angiography revealed a left dominant system. For these patients, both the inferior and lateral walls were ascribed to the left circumflex vessel. The apex was allocated to any other involved territory. If, however, the apex alone was involved, the LAD was implicated.

## RESULTS

### Physical Measurements

The modification of the dual-head SPECT camera resulted in an extension of the linear energy range to 511 keV with no alteration in performances at the low-energy range. The integral uniformity in both regions was measured to be  $<6\%$ .

Planar spatial resolution measurements in air for the UHE collimator with  $^{18}\text{F}$  and  $^{99m}\text{Tc}$  and the LEHR collimator with  $^{99m}\text{Tc}$  are summarized in Table 1 along with the system plane source sensitivity measurements. By evaluating detected counts outside a 10-cm diameter circular region of interest over the disk source of  $^{18}\text{F}$  and contributions to line spread measurements from penetration, it was estimated that approximately 52% of the detected photons were due to penetration. Therefore, excluding penetration, the system sensitivity for  $^{18}\text{F}$  was calculated to be 62 cpm/ $\mu\text{Ci}$ . Planar system spatial resolution measurements indicated that the spatial resolution for  $^{99m}\text{Tc}$  was superior to that for  $^{18}\text{F}$  using the UHE collimator. The spatial resolution for  $^{99m}\text{Tc}$ , however, was inferior to that routinely obtained with the high-resolution collimator.

SPECT spatial resolution measurements with scatter yielded measurements of 14.5 mm and 17.0 mm for  $^{99m}\text{Tc}$  and  $^{18}\text{F}$ , respectively, for the UHE collimator. SPECT volume sensitivity measurements yielded values of 125 cpm/ $\mu\text{Ci}$  and 270 cpm/ $\mu\text{Ci}$  for  $^{99m}\text{Tc}$  and  $^{18}\text{F}$ , respectively. The

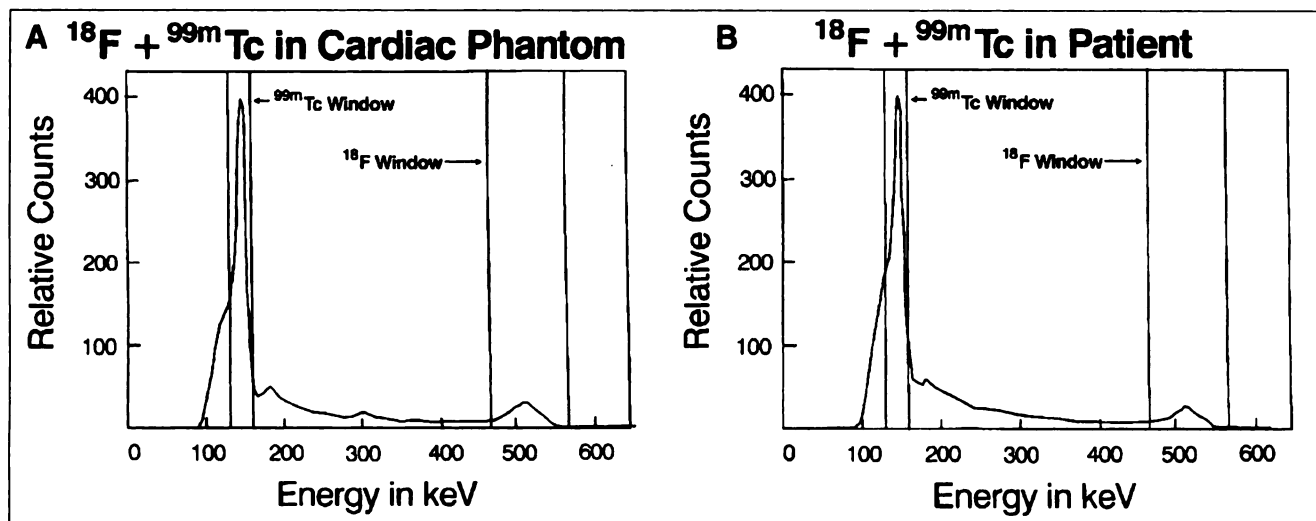


**FIGURE 4.** (A) Energy spectrum obtained with a scintillation camera in the anterior position from a cardiac phantom containing a solution of  $^{99m}\text{Tc}$  and  $^{18}\text{F}$  in a 3.2:1 concentration ratio, and (B) energy spectrum obtained in the anterior position with a scintillation camera from a patient just before the start of the acquisition of the DISA-SPECT protocol.

increased  $^{18}\text{F}$  sensitivity for SPECT (compared to  $^{99m}\text{Tc}$ ) is due to the colinear emission of two 511 keV photons from each positron annihilation coupled with the dual detector,  $180^\circ$  geometry. The high septal penetration of  $^{18}\text{F}$  and less attenuation effects are also contributing factors.

By using a cardiac phantom, a comparison of reconstructed images from the single anterior detector of the dual-head SPECT system ( $180^\circ$  acquisition) versus both detectors together ( $360^\circ$  acquisition) showed that the image quality was slightly superior for the single-head acquisition. Images from the SPECT camera with the UHE collimator demonstrated that  $^{18}\text{F}$ FDG-SPECT can resolve cold defects of  $2 \times 0.5$  cm in the heart (20).

The cardiac phantom containing  $^{18}\text{F}$  alone was imaged with DISA-SPECT. Images were obtained from the  $^{18}\text{F}$  and  $^{99m}\text{Tc}$  windows. These images were normalized to the pixel containing the maximum number of counts in the  $^{18}\text{F}$  window. Measurements of total counts from the heart phantom in the two windows indicated that downscatter into the  $^{99m}\text{Tc}$  window was 31% of the counts recorded in the  $^{18}\text{F}$  window. Images were then obtained from the  $^{99m}\text{Tc}$  window after adding a solution of  $^{99m}\text{Tc}$  to the phantom in a concentration 3.2 times that of  $^{18}\text{F}$ . These images were normalized to the maximum pixel counts in the  $^{99m}\text{Tc}$  window. The high quality of the reconstructed images was evident for both the  $^{18}\text{F}$  and  $^{99m}\text{Tc}$  windows with both simulated lesions being clearly defined. The two datasets also clearly indicated the direct image comparison capability, due to the 1:1 correspondence of comparable slices, provided by the dual-isotope imaging technique. By measuring the total counts in the  $^{99m}\text{Tc}$  window from the cardiac phantom and assuming that 31% of the counts from the  $^{18}\text{F}$  peak appears in the  $^{99m}\text{Tc}$  window, it was determined that only 5.9% of the counts in the  $^{99m}\text{Tc}$  window were due to downscatter from  $^{18}\text{F}$ . An energy spectrum from  $^{99m}\text{Tc}$  and  $^{18}\text{F}$  in the 3.2:1 concentration ratio was measured with the camera in

the anterior position and clearly indicated the ability to resolve the  $^{99m}\text{Tc}$  photopeak from the other structures in the spectrum (Fig. 4A).

Total counts from the heart were determined for the two energy windows in five patients imaged with the dual-isotope protocol. All patients were reported as having normal distributions of the two radiopharmaceuticals and normal coronary angiograms. Assuming 31% downscatter from  $^{18}\text{F}$  as measured from the phantom study, the average contribution to the  $^{99m}\text{Tc}$  window was measured to be between 3.7%–6.6% of the total count measured in the  $^{99m}\text{Tc}$  window for the patients with normal global perfusion and metabolism. An energy spectrum from a patient with the camera in the anterior position over the patient's chest is shown in Figure 4B. This spectrum is virtually identical to that of the phantom in Figure 4A, and thus confirms the predicted 3.2:1 ratio of  $^{99m}\text{Tc}$  to  $^{18}\text{F}$  at the time of imaging for normal patients.

In imaging situations where global perfusion is reduced and/or metabolism is increased, the percentage contribution of  $^{18}\text{F}$  downscatter to  $^{99m}\text{Tc}$  will be greater than 5.9% and may affect the visual evaluation of an area of ischemia. Figure 5 shows the results of the sample counting experiment to evaluate this effect. For the four global perfusion rates chosen (normal to 25% normal), five datasets representing 100% to 0% ischemia (0%–100% contrast ratio) were evaluated. In each of these cases, the effect of  $^{18}\text{F}$  downscatter was calculated from the sample data for a range of up to four times the activity representing normal metabolism. For this experiment,  $100 \mu\text{Ci}$   $^{18}\text{F}$  represents normal metabolism and  $320 \mu\text{Ci}$   $^{99m}\text{Tc}$  represents normal perfusion, i.e. 3.2:1. The range of percent contrast values [(ischemic region/normal myocardium)  $\times$  100] based on  $^{99m}\text{Tc}$  window counts] shown in each of the graphs demonstrate the effect of increased metabolism (up to four times normal) along with each of the global perfusion rates

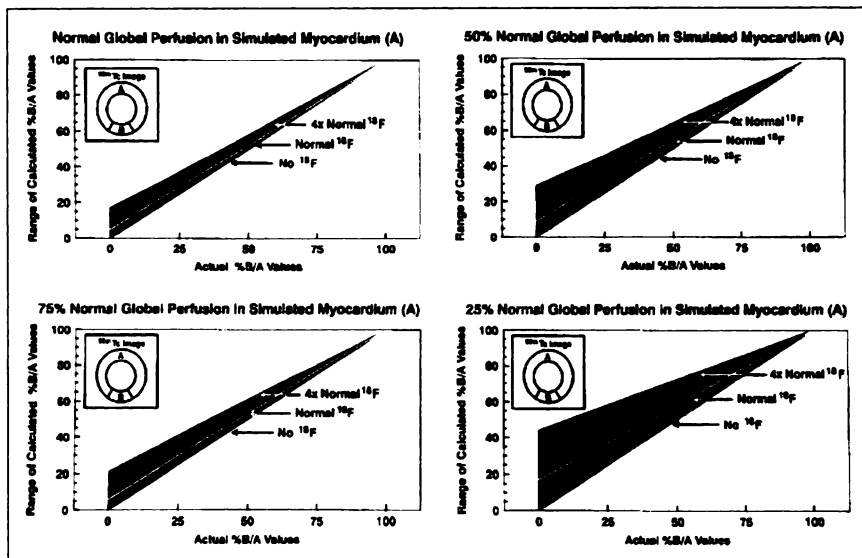


**FIGURE 5.** Effect of  $^{18}\text{F}$  downscatter on image contrast. The range of calculated values of percent contrast ( $^{99\text{m}}\text{Tc}$  window counts in ischemic region (B) /  $^{99\text{m}}\text{Tc}$  window counts in normal area (A)  $\times 100$ ) are plotted versus actual contrast as determined by ratios of activities of  $^{99\text{m}}\text{Tc}$  in (A) and (B). Each graph shows the range of values obtained for the global perfusion rate indicated in the presence of zero to four times normal metabolism. For example, in the first graph, an area of 100% ischemia (% B/A = 0) would produce a range of contrast measurements of 0% to 20% in the presence of zero to four times normal metabolism due to  $^{18}\text{F}$  downscatter in the  $^{99\text{m}}\text{Tc}$  window. Note that 0% to 100% B/A corresponds to 100% to 0% ischemia.

chosen for this demonstration. These values in each range can be compared to the minimum values, which are the actual values determined by the ratio of  $^{99\text{m}}\text{Tc}$  activities in the two samples and to the values for normal metabolism indicated by the white line. The increases over the actual values are due to  $^{18}\text{F}$  downscatter into the  $^{99\text{m}}\text{Tc}$  window.

### Clinical Analysis

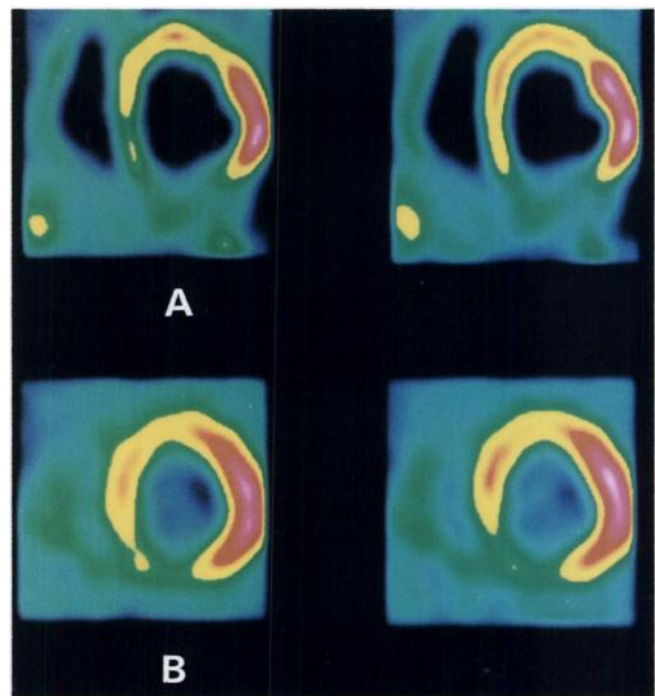
Although the images obtained from the LEHR collimator demonstrated superior resolution, the diagnostic information was equivalent and independent of whether the studies were obtained with either the LEHR or the UHE collimator in the four patients who underwent the modified protocol (Fig. 6).

Table 2 shows the clinical and imaging data of the 15 patients who underwent the rest DISA-SPECT protocol. Five patients had only mismatched defects indicative of ischemia, seven had only matched defects indicative of scar and two had both matched and mismatched defects. Typical patients with matched and mismatched defects are shown in Figures 7 and 8, respectively.

Table 3 shows the correlation between  $^{99\text{m}}\text{Tc}$ -MIBI/ $^{18}\text{F}$ FDG scintigraphy and angiography in the 14 patients who underwent coronary angiography. The seven patients with a matched defect had a recent documented inferior myocardial infarction. Five patients had only mismatched defects. Of these five patients, one had no documented history of CAD and four had known CAD. The one patient with a mismatched defect (anterior wall) and no significant CAD on angiography (false-positive) had no previously documented infarction and the coronary angiogram revealed no significant stenoses in the coronary arteries. There was mild decreased  $^{99\text{m}}\text{Tc}$ -MIBI uptake in the inferior wall with normal  $^{18}\text{F}$ FDG distribution. This was interpreted as a mismatch suggestive of mild ischemia of the inferior wall. The mismatched defect could be secondary to diaphragmatic attenuation on the  $^{99\text{m}}\text{Tc}$ -MIBI scan and no attenuation was seen on the  $^{18}\text{F}$ FDG scan (higher energy with better

penetration through the diaphragm). The echocardiography and left ventriculogram, however, revealed global hypokinesis (EF = 48%) with akinesis of the inferior wall.

The remaining four patients with only mismatched defects had angiographic stenosis corresponding to the regional distributions of these defects. One patient with both matched and mismatched defects had documented myocardial infarction with wall motion abnormalities on the left ventriculogram and evidence of ischemia in the same vas-



**FIGURE 6.** An 82-yr-old man with ischemic cardiomyopathy. Technetium-99m MIBI short-axis images of the heart acquired with the (A) LEHR and (B) UHE collimators that provide similar diagnostic information, showing a large area of decreased perfusion in the septum and inferior wall of the left ventricle (arrow).

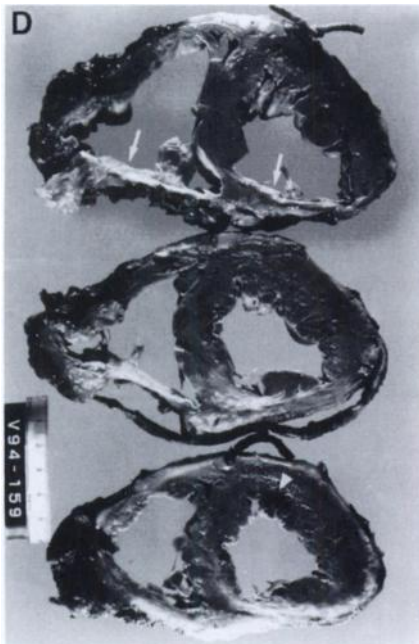
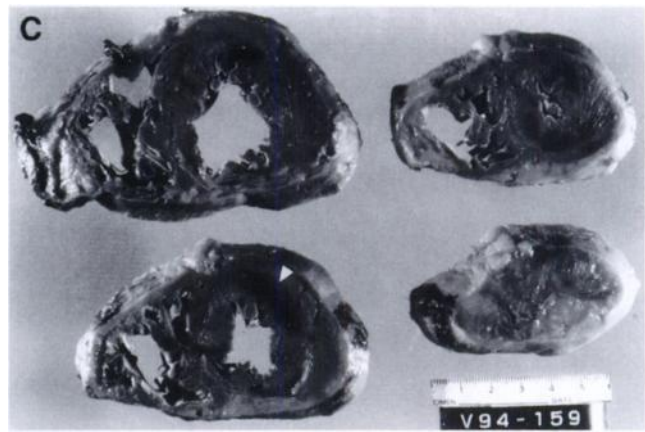
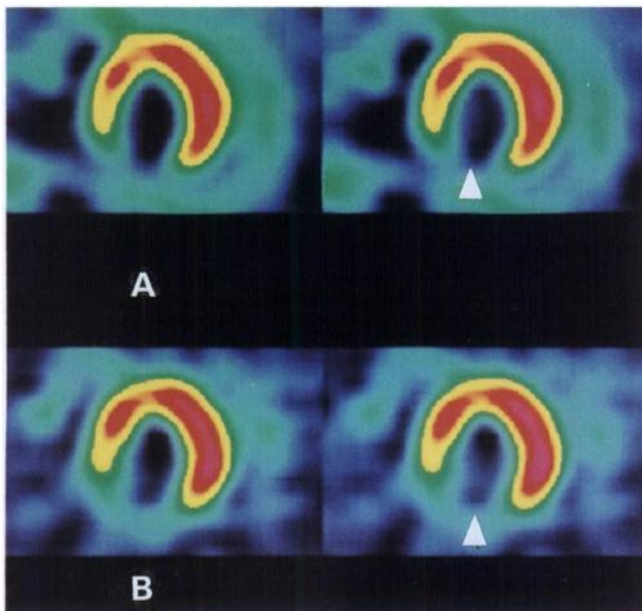


**FIGURE 7.** A 59-yr-old man with a history of severe triple-vessel disease. The patient died soon after undergoing the  $^{99m}\text{Tc}$  MIBI/ $^{18}\text{F}$ FDG scan from an acute myocardial infarction. (A) Technetium- $^{99m}$ -MIBI and (B)  $^{18}\text{F}$ FDG SPECT short-axis images identify an area of myocardial scar in the inferior wall. (C,D) Autopsy specimen demonstrates an old transmural myocardial infarct in the inferior wall (arrows) extending into the right ventricle and an acute anterior myocardial infarction (arrowheads).

cular distribution as the prior myocardial infarction. The other patient with both matched and mismatched defects had no prior documented myocardial infarction but severe aortic stenosis. The defects on this patient's DISA-SPECT scan correlated with the lesions seen on coronary angiogram.

One-hundred twenty-six segments were analyzed and the distribution of the segmental uptake pattern (normal, matched defects and mismatched defects) according to the three individual coronary arteries is represented in Figure 9 for the patients who underwent coronary angiography ( $n = 14$ ). Analysis of the correlation of scintigraphic assessment according to the three individual coronary artery distributions revealed 100% correlation in the LAD and circumflex artery distribution, although the number of diseased seg-

ments in the circumflex distribution is limited. The one false-positive scan was in the RCA distribution, but angiography showed no evidence of RCA stenosis despite the presence of a mismatched defect on the  $^{99m}\text{Tc}$ -MIBI/ $^{18}\text{F}$ FDG scan.

The interpretation by the two independent observers agreed in 97% (122/126) of the segments. In all the patients, the disagreement was related to defect extent but not to the vascular territory involved.

In the 14 patients who had coronary angiography, the sensitivity of  $^{99m}\text{Tc}$ -MIBI/ $^{18}\text{F}$ FDG DISA-SPECT for detecting CAD was 100%, with a positive predictive value of 93%. The specificity and negative predictive value could not be calculated in the absence of true-negative patients.

**TABLE 3**  
Correlation between Technetium-99m-MIBI/Fluorine-18-Scans and Angiography

	Angiography-Negative	Angiography-Positive	Total
Normal	0TN	0FN	0
Mismatched defects only	1FP	4TP	5
Matched defects only	0FP	7TP	7
Mismatched and matched defects	0 F	2	2
Total	1	13	14

TN = true-negative; FN = false-negative; TP = true-positive; FP = false-positive.

## DISCUSSION

According to recent studies, gamma cameras equipped with UHE collimators can provide  $^{18}\text{F}$ FDG images of sufficient quality to permit accurate clinical diagnosis in patients with suspected ischemic heart disease (19,20). Previous work in our laboratory has demonstrated the ability of the modified Apex dual-head Helix (Elscent, Inc.) fitted with UHE collimators to provide excellent SPECT quality images of the heart using  $^{18}\text{F}$ FDG compared to  $^{18}\text{F}$ FDG-PET (20). Burt et al. compared  $^{18}\text{F}$ FDG-PET and  $^{18}\text{F}$ FDG-SPECT to resting  $^{201}\text{Tl}$  cardiac images and found that  $^{18}\text{F}$ FDG-PET and SPECT were superior to  $^{201}\text{Tl}$  at detecting viable myo-

cardium (21). Oppenheim et al. compared 66 regions in 10 patients by both  $^{18}\text{F}$ FDG-PET and  $^{18}\text{F}$ FDG-SPECT, and, although they acknowledged that  $^{18}\text{F}$ FDG-PET images had better resolution and in several cases more prominently identified the defect, they found that  $^{18}\text{F}$ FDG-SPECT images provided sufficient diagnostic clinical information (22). Bax et al. examined 15 patients with regional wall motion abnormalities identified by two-dimensional echocardiography prior to CABG or percutaneous transluminal coronary angioplasty. Each patient underwent both  $^{18}\text{F}$ FDG-SPECT during hyperinsulinemic clamping and resting  $^{201}\text{Tl}$  imaging to evaluate the presence of viable myocardium prior to revascularization. A two-dimensional echocardiogram was performed postrevascularization. Regional wall motion abnormalities improved in 77% of the mismatched regions, and 89% of the matched regions showed no change in wall motion (23). Double-acquisition cardiac studies to evaluate hibernating myocardium with  $^{18}\text{F}$ FDG-SPECT/ $^{201}\text{Tl}$  or  $^{99\text{m}}\text{Tc}$ -MIBI SPECT have been performed and reportedly provide comparable images and adequate clinical information as compared to  $^{13}\text{N}$ -ammonia/ $^{18}\text{F}$ FDG-PET (20–23).

This study evaluated the feasibility of DISA-SPECT imaging with  $^{99\text{m}}\text{Tc}$ -MIBI and  $^{18}\text{F}$ FDG to identify injured but viable myocardium. The design of this study is similar to that recently described by Stoll et al. who have reported their experience using  $^{99\text{m}}\text{Tc}$ -MIBI/ $^{18}\text{F}$ FDG and DISA-SPECT in a series of 30 patients with cardiac disease (24). Significant differences between the two studies include the superior resolution of the images generated in our study and the ability to demonstrate that these images were capable of providing equivalent diagnostic information when compared to  $^{18}\text{F}$ FDG cardiac PET (20). The difference in image resolution is most likely related to the digital tech-

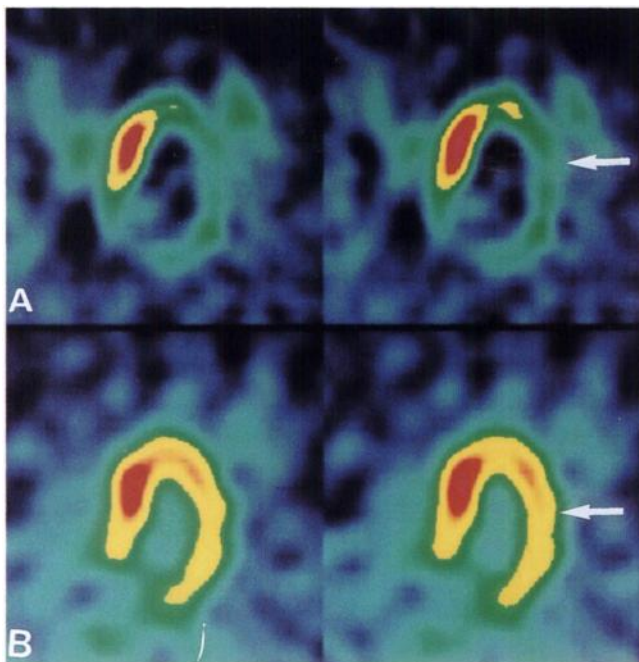


**FIGURE 8.** A 43-yr-old woman with a brief history of CAD. (A) Technetium-99m-MIBI and (B)  $^{18}\text{F}$ FDG DISA-SPECT horizontal long-axis images of the heart show a large area of diminished perfusion and maintained metabolism in the lateral wall (arrow), indicating ischemic but viable myocardium.

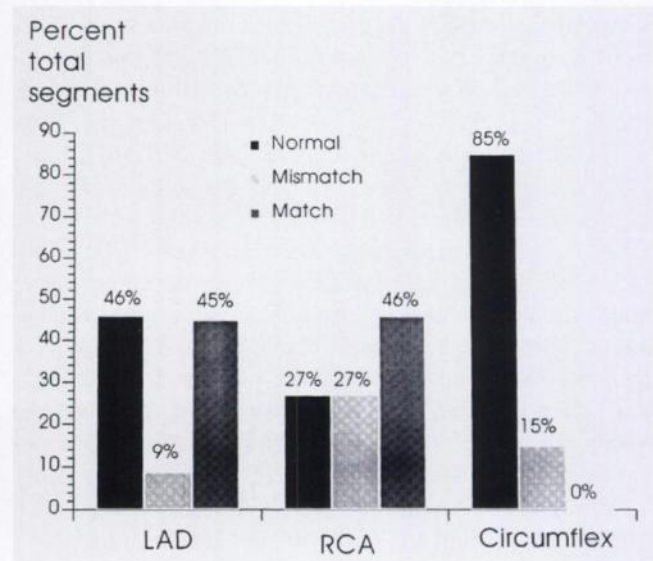


**FIGURE 9.** Distribution of the segmental pattern of uptake according to coronary artery distribution is depicted for patients who had angiography ( $n = 14$ ). There are a total of 126 segments (LAD = 70 segments, RCA = 28 segments, circumflex = 28 segments).

nology utilized by the Apex dual-head Helix, which permits an extension of the energy range of the camera with excellent uniformity and linearity.

#### Advantages of Rest Technetium-99m-MIBI/Fluorine-18-FDG DISA-SPECT

The advantages of a simultaneous acquisition protocol include patient convenience, shorter image acquisition time and perfect image registration. The larger axial field of view of most gamma cameras (40 cm for the Apex Helix) as compared to PET (13–15 cm) is a relative advantage when imaging patients with cardiomegaly. In addition, since imaging is performed with  $^{18}\text{F}$ FDG, there is no need for patients to undergo 24-hr imaging, as is recommended for fixed defects after  $^{201}\text{Tl}$  reinjection to evaluate hibernating myocardium (18). The cost-effectiveness of identifying injured but viable myocardium with DISA SPECT is related to multiple issues. First, PET is infrequently used to identify hibernating myocardium because of its limited availability and high cost. Second, the acquisition of a third set of images due to the presence of a fixed defect after  $^{201}\text{Tl}$  re-injection to identify hibernating myocardium increases the technical cost of the  $^{201}\text{Tl}$  study and may also delay the patient's discharge, which further increases cost. The protocol described in this study requires a single SPECT acquisition, resulting in decreased technical fees which help offset the cost of  $^{18}\text{F}$ FDG.

#### Limitations

A potential limitation of using  $^{18}\text{F}$ FDG includes patients with diabetes or a prediabetic condition. Although administration of soluble insulin improves myocardial  $^{18}\text{F}$ FDG uptake, a significant number of patients with diabetes or a prediabetic condition continue to demonstrate poor myocardial  $^{18}\text{F}$ FDG uptake. Implementation of the euglycemic hyperinsulinemic clamp described by Knuuti et al. (25) to stimulate myocardial glucose utilization prior to  $^{18}\text{F}$ FDG-SPECT imaging has resulted in excellent image quality in insulin-dependent diabetic patients studied in our laboratory.

The difference in attenuation between  $^{99\text{m}}\text{Tc}$ -MIBI and  $^{18}\text{F}$ FDG, especially by the diaphragm, should be recognized as a potential source of false-positive studies with DISA-SPECT. In our experience, attenuation of  $^{18}\text{F}$ FDG with DISA-SPECT has been insufficient to cause false-positive metabolic studies. We are presently developing a method of attenuation correction for  $^{99\text{m}}\text{Tc}$ -MIBI in DISA-SPECT imaging. As a temporary solution, patients are imaged in the prone position, whenever possible, to minimize the number of false-positive studies with DISA-SPECT secondary to diaphragmatic attenuation.

Experimental data from this study using simulated myocardial distributions of  $^{99\text{m}}\text{Tc}/^{18}\text{F}$  revealed that the downscatter contribution from  $^{18}\text{F}$  into the  $^{99\text{m}}\text{Tc}$  image becomes theoretically significant in regions of severe ischemia (75%–100%), with a fourfold increase in metabolism when associated with a twofold decrease in global perfusion.

#### CONCLUSION

Although these preliminary data need to be confirmed with a larger series of patients and outcome monitoring,  $^{99\text{m}}\text{Tc}$ -MIBI/ $^{18}\text{F}$ FDG DISA-SPECT may become the protocol of choice for evaluating injured but viable myocardium due to its availability, logistics, patient convenience and cost-effectiveness.

#### ACKNOWLEDGMENTS

The authors thank Virginia Brocker for preparing the manuscript, John Bobbitt for preparing the images and Joey Forrester for technical assistance.

#### REFERENCES

1. Tillisch J, Brunken R, Marshall R, et al. Reversibility of cardiac wall motion abnormalities predicted by positron tomography. *N Engl J Med* 1986;314:884–888.
2. Tamaki N, Yonekura Y, Yamashita K, et al. Positron emission tomography using fluoro-18 deoxyglucose in evaluation of coronary artery bypass grafting. *Am J Cardiol* 1989;64:860–865.
3. Nienaber CA, Brunken RC, Sherman CT, et al. Metabolic and functional recovery of ischemic human myocardium after coronary angioplasty. *J Am Coll Cardiol* 1991;18:966–978.
4. Marwick TH, Nemecek JJ, Lafont A, Salcedo EE, MacIntyre WJ. Prediction by postexercise fluoro-18-deoxyglucose positron emission tomography of improvement in exercise capacity after revascularization. *Am J Cardiol* 1992;69:854–859.
5. Lucignani G, Paolini G, Landoni C, et al. Presurgical identification of hibernating myocardium by combined use of technetium-99m hexakis 2-methoxyisobutylisonitrile single photon emission tomography and fluorine-18 fluoro-2-deoxy-D-glucose positron emission tomography in patients with coronary artery disease. *Eur J Nucl Med* 1992;19:874–881.
6. Carrel Y, Jenni R, Haubold-Reuter S, Schulthess G, Pasic M, Turina M. Improvement of severely reduced left ventricular function after surgical vascularization in patients with preoperative myocardial infarction. *Eur J Cardiothorac Surg* 1992;6:479–484.
7. Eitzman D, Al-Aouar Z, Kanter HL, et al. Clinical outcome of patients with advanced coronary artery disease after viability studies with positron emission tomography. *J Am Coll Cardiol* 1992;20:559–565.
8. Louie HW, Laks H, Milgater E, et al. Ischemic cardiomyopathy. Criteria for coronary revascularization and cardiac transplantation. *Circulation* 1991;84:III290–III295.
9. Rahimtoola SR. The hibernating myocardium. *Am Heart J* 1989;117:211–221.
10. Kiat H, Berman DS, Maddahi J, et al. Late reversibility of tomographic myocardial thallium-201 defects: an accurate marker of myocardial viability. *J Am Coll Cardiol* 1988;12:1456–1463.
11. Rocco TP, Dilsizian V, McKusick KA, Fishman AJ, Strauss HW. Comparison of thallium redistribution with "rest/reinjection" imaging for the detection of viable myocardium. *Am J Cardiol* 1990;66:158–163.
12. Dilsizian V, Rocco TP, Freedman NMT, Len MB, Bonow RO. Enhanced detection of ischemic but viable myocardium by the reinjection of thallium after stress-redistribution imaging. *N Engl J Med* 1990;323:141–146.
13. Tamaki N, Ohtani H, Yonekura Y, et al. Significance of fill-in after thallium-201 reinjection following delayed imaging: comparison with regional wall motion and angiographic findings. *J Nucl Med* 1990;31:1617–1623.
14. Ohtani H, Tamaki N, Yonekura Y, et al. Value of thallium-201 reinjection after delayed SPECT imaging for predicting reversible ischemia after coronary artery bypass grafting. *Am J Cardiol* 1990;66:394–399.
15. Tamaki N, Ohtani H, Yamashita K, et al. Metabolic activity in areas of new fill-in after thallium-201 reinjection: comparison with positron emission tomography using fluorine-18-deoxyglucose. *J Nucl Med* 1991;32:673–678.
16. Brunken RC, Mody FV, Hawkins RA, Nienaber C, Phelps ME, Schelbert HR. Positron emission tomography detects metabolic activity in myocardium with persistent 24-hour single photon emission computed tomography thallium-201 defects. *Circulation* 1992;86:1357–1369.
17. Williams KA, Taillon LA, Stark VJ. Quantitative planar imaging of glucose metabolic activity in myocardial segments with exercise thallium-201 perfusion defects in patients with myocardial infarction: comparison with late

- (24-hour) redistribution thallium imaging for detection of reversible ischemia. *Am Heart J* 1992;124:294–303.
18. Woods RC, Martin WH, Delbeke D, Sandler MP. Prognostic value of delayed 24-hour SPECT after high dose thallium-201 stress-reinjection imaging [Abstract]. *Eur J Nucl Med* 1994;21:S79.
  19. Drane WE, Abbott FD, Nicole MW, Mastin ST, Kuperus JH. Technology for FDG-SPECT with a relatively inexpensive gamma camera. *Radiology* 1994;191:461–465.
  20. Martin WH, Delbeke D, Patton JA, et al. FDG-SPECT: correlation with <sup>18</sup>F-DG-PET. *J Nucl Med* 1994;36:988–995.
  21. Burt RW, Perkins OW, Oppenheim BE, et al. Comparison of rest-thallium SPECT, F-18-FDG PET and F-18-FDG SPECT for evaluation of myocardial viability [Abstract]. *J Nucl Med* 1994;35(suppl)49P.
  22. Oppenheim BE, Burt RW, Schauwecker DS. Comparison of a three detector gamma camera and a PET scanner for performing F-18-FDG cardiac scintigraphy [Abstract]. *J Nucl Med* 1994;35(suppl):111P.
  23. Bax JJ, Cornel JH, Visser JC, Fioretti PM, et al. Reversibility of wall motion abnormality by SPECT with F-18-fluorodeoxyglucose [Abstract]. *J Nucl Med* 1994;35(suppl):136P.
  24. Stoll HP, Hellwig N, Alexander C, Ozbek C, Schieffer H, Oberhausen E. Myocardial metabolic imaging by means of fluorine-18 deoxyglucose/technetium-99m sestamibi dual-isotope single-photon emission tomography. *Eur J Nucl Med* 1994;21:1085–1093.
  25. Knuuti MJ, Nuutila P, Ruotsalainen U, et al. Euglycemic hyperinsulinemic clamp and oral glucose load in stimulating myocardial glucose utilization during positron emission tomography. *J Nucl Med* 1992;33:1255–1262.